JOURNAL OF CATALYSIS **167,** 379–390 (1997)
ARTICLE NO. CA971583

Strong Metal–Promoter Oxide Interactions Induced by Calcination in V, Nb, and Ta Oxide Promoted Rh/SiO_2 Catalysts

T. Beutel,*,[1] V. Siborov,† B. Tesche,‡ and H. Knözinger*

*Institut für Physikalische Chemie, Sophienstrasse 11, 80333 München, Germany; †Boreskov Institute of Catalysis, Prospekt Akademika Lavrentieva 5, Novosibirsk 690090, Russia; and ‡Max-Planck-Institut für Kohleforschung, Kaiser-Wilhelm-Platz 1, 45470 Mülheim, Germany

Received September 26, 1996; accepted December 5, 1996

The influence of the calcination temperature on the structure of Rh/SiO_2 catalysts promoted by Vb transition metal oxides has been studied. Calcination at $T > 973$ K leads to the formation of crystalline $RhXO_4$ mixed oxides with increasing abundance in the order $RhTaO_4 < RhNbO_4 < RhVO_4$. Their reduction at $T = 773$ K yields highly dispersed Rh° metal particles which seem to be embedded in a matrix of partially reduced promoter oxide. The presence of Vb metal oxides enhances the noble metal dispersion as compared to unpromoted Rh/SiO_2 catalysts. Calcination at $T = 773$ K establishes an interaction between Rh_2O_3 and promoter oxide which manifests itself in a decreased CO-chemisorption capacity after low temperature reduction (LTR = 523 K). This calcination induced metal–promoter interaction decreases with increasing atomic number of the promoter element.

INTRODUCTION

Metal–promoter interactions can be classified by the dimension of the interface and by the nature of the metal–promoter bond at the interface. The contact between metal and promoter may be zero-, one-, or two-dimensional. Zero-dimensional interactions occur in metal clusters which are anchored to cus promoter sites (1) or protons (2). The coverage of edges or faces of metal particles by promoter can accordingly be considered two- and three-dimensional interactions, respectively.

Most relevant for catalysis are those interactions which allow reactants to interact simultaneously with metal and promoter. In the case of metal particles covered by patches of promoter oxide, some steps in the overall reaction mechanism may be catalyzed at the metal–promoter–gas/liquid interphase. The creation of a metal–promoter perimeter has been proven pivotal to catalytic properties, such as ethane hydrogenolysis (3) or CO hydrogenation reactions (4–8).

Depending on the state of the promoter, the nature of the metal–promoter interaction can be of the van der Waals type with polarization of metal atoms or clusters (1, 9, 10). If chemical bonds are established between metal and promoter, charge transfer can occur if the Fermi levels of the phases in contact are different (11, 12). This may generate electron deficient or electron rich metal particles.

The strength of the metal promoter interaction is more difficult to address. The heat of formation of metal–promoter bonds can usually only be estimated. Recent calculations on metal–proton adducts, Pd_4H^+, which exist in Pd/HY zeolite, show that the deprotonation energy of the protonated metal cluster is comparable to that of NH_4^+ cations (13).

The most common procedure for achieving metal–promoter interactions in M/XO_y systems consists in a high temperature reduction ($T > 673$ K). This leads to a strong decrease of the CO or H_2 chemisorption capacities of the supported noble metal catalysts. The phenomenon was discovered in 1978 by Tauster *et al*. who called it strong metal support interaction (SMSI) (14, 15). The chemisorption capacity can be restored by oxidation and subsequent low temperature (LT) reduction ($T < 473$ K). This effect does not occur with MgO, Al_2O_3, or SiO_2, but only with reducible oxides, such as TiO_2, MnO_2, V_2O_5, or Nb_2O_5. The effect is also observed in noble metal catalysts which are supported by an inert material but promoted by transition metal oxides and is referred to as SMPI (strong metal promoter interaction) in this paper. It is generally agreed upon that the SMPI effect is caused by a decoration of the noble metal surface by promoter oxide patches (16–22). It has been stated that the support or promoter oxide are partially reduced in the SMSI and SMPI state, respectively.

Since then was the chemisorption capacity of the metal related to the strength of the metal–promoter interaction. However, reduced H_2 chemisorption capacities are also observed for metal clusters which are anchored to protons in zeolite cages (23). No HT (high temperature) reduction is required in this case and the strength and nature of the interaction are probably very different from those of the classical SMSI state.

[1] Present address: Laboratoire de Réactivité de Surface, 1106 URA du CNRS, Université P. et M. Curie, 4 Place Jussieu, 75252 Paris Cedex05, France.

0021-9715/97 $25.00

Another route for increasing metal–promoter oxide interactions consists in high temperature calcinations followed by HT reduction. In the latter case mixed oxides are formed as precursors during HT calcination which are transformed into metal particles and suboxides of the respective transition metal in the following reduction step. With Rh as the noble metal component, supported mixed oxides have been found with oxides of W (24, 25), Mo (24, 25), Mn (25), Cu (26), V (26), or Nb (27). Alloys were formed upon reduction of $MoRh_2O_6$ and WRh_2O_6, but metal particles incapsulated in a matrix of reduced promoter oxide are found with other transition metal oxides. This is the first comparative study of the formation and reduction of ternary oxides of Rh and Vb transition metals supported on silica. We will report in a separate paper that the oxoselectivity in CO hydrogenation reactions depends on the way of inducing metal–promoter interactions, that is if the HT reduction is preceeded by a calcination pretreatment or not.

The HT reduction results mostly in a partial reduction of the promoter oxide phase, and the reduced oxidation state of the promoter is generally considered a necessary condition in achieving the SMPI state. Recent XPS studies on Rh/TiO_2 model systems, however, show that SMPI effects can be induced by heat treatments in UHV (28). In contrast to the H_2 induced SMSI effect, no Ti^{3+} ions were detected by XPS.

In this paper we will present a new method of introducing metal promoter oxide interactions without reducing the catalyst at high temperatures. This method consists in calcination at the onset temperature of bulk mixed oxide formation followed by LT (low temperature) reduction.

EXPERIMENTAL

Sample Preparation

Promoted Rh/SiO_2 catalysts were prepared by stepwise impregnation of precalcined silica (Alpha Products, 330 m^2/g, $T_{calc} = 773$ K) with an aqueous solution of NH_4VO_3 (Fluka, >99%) + oxalic acid (Merck, >99%), niobic acid ($Nb_2O_5 \cdot H_2O$, CBMM, AD/620) + oxalic acid, and a commercial tantalum oxalate solution (HCST, 145 g, Ta_2O_5/liter). The suspensions were stirred for 1 h at room temperature (rt) prior to evaporation of the solvent at a pressure of 25 hPa and $T = 333$ K. Samples were then dried in air at 383 K for 12 h, ground in an agate mortar, and calcined to 773 K for 3 h in order to decompose Vb–metal oxalate complexes.

These materials were thereafter impregnated with an aqueous solution of $Rh(NO_3)_3$. Removal of water and subsequent drying were performed analogously to the first impregnation step. The samples were then submitted to a 7-h calcination at 573, 773, 973, and 1173 K, respectively. The resulting catalysts are denoted Rh/*X*/573, Rh/*X*/773, Rh/*X*/973, and Rh/*X*/1173, respectively, with X = V, Nb, Ta. The nominal Rh loading is 3 wt%, the ratio $X : Rh = 4$ for all promoted Rh/SiO_2 catalysts.

As reference substances, unpromoted Rh/SiO_2 catalysts were prepared following the recipe described above. These samples are accordingly denoted Rh/573, Rh/773, Rh/973, and Rh/1173, and contain 3 wt% Rh.

Experimental Methods

Specific surface area measurements were performed on a Quantasorb. Samples were pretreated for 1 h at 383 K in a flow of N_2 (Linde 5.0), before measuring N_2 adsorption isotherms with mixtures of 10, 20, and 30% N_2 in He.

X-ray diffraction (XRD) experiments were carried out in reflection using an HTK-10 Anton Paar high temperature chamber attached to a Siemens D 500 diffractometer. Monochromatized Cu$K\alpha_1$ radiation was used. *In situ* diffraction patterns were taken of the calcined catalysts and after reduction in 5% H_2 (balance He) for 1 h.

For temperature programmed reduction (TPR), samples were pretreated in a flow of N_2 for 1 h in order to remove physisorbed water before being weighed. A mixture of 5% H_2 (Linde 5.0) in N_2 was applied at a total flow rate of 10 ml/min and a heating ramp of 10 K/min using 50 mg of sample. H_2 consumptions were registered by a thermal conductivity detector (TCD); the accuracy of the quantitative evaluation of peak areas was ±5%.

CO chemisorption capacities were determined on a Micromeritics Pulse Chemisorb 2700 sorptometer in a pulse flow mode. In order to remove hydrocarbon impurities, catalysts were treated in O_2 (Linde 4.5) at 573 K for 20 min. Samples were then reduced *ex situ* in flowing H_2 (50 ml/min) at 473 K for 1 h at 523, 673, or 773 K at a heating rate of 5 K/min. After flushing with N_2 for 15 min at the respective temperature of reduction, the sample was cooled to 300 K and sealed in a glass tube. For CO chemisorption measurements, 50 mg of the sealed catalyst were transferred into a reactor and attached to the sorptometer. Prior to exposure of CO, catalysts were reduced *in situ* in flowing H_2 (20 ml/min) for 30 min (heating rate, 30 K/min). CO uptakes were measured at 300 K by repeated injection of 70-μl pulses of CO (Linde 3.0) into flowing H_2 (20 ml/min) carrier gas until saturation was reached (29). The sensitivity of detection of chemisorbed CO was in the range 3–4 μl CO per gram catalyst.

For FTIR spectroscopy, samples were pressed at 10^7 Pa into self-supporting wafers of 10–15 mg per cm^2. Spectra were recorded in transmission on a Bruker IFS66 FTIR spectrometer at a resolution of 2 cm^{-1}. Sixty-four scans were accumulated using an MCT detector. Spectra are corrected for background absorbance and the mass exposed to the beam (see below). Wafers were placed in a copper cell, described earlier (30), which was sealed with CaF_2 windows and could be evacuated to 10^{-5} hPa. Catalysts

were pretreated *in situ* in O_2 (Linde 4.5) at 573 K in order to clean the surface from hydrocarbon contaminations. Subsequent reduction was performed in a flow of H_2 (Linde 5.0) at a flow rate of 50 ml/min and a heating ramp of 5 K/min starting at 333 K. H_2 treatments were carried out at 673 K for 2 h. After evacuation of the samples for 1 h at the respective temperature of reduction, catalysts were cooled to 85 K and exposed to CO.

Transmission electron microscopy (TEM) was carried out on a Siemens Elmiscop 102 operated at 100 keV. An electron-optical magnification of 120,000 : 1 was chosen. The diffraction length was 700 nm and calibrated with thallium chloride. For TEM investigations, powder materials were placed onto a carbon film of 4 nm thickness, which covered Cu grids of 60 mesh width. The catalyst powders were suspended ultrasonically in ethanol, and a drop of the resulting suspension was deposited on the carbon film. The remaining solvent was removed after 1 min.

RESULTS

Oxidized State

The specific surface areas of the Rh/X/SiO_2 samples are compiled in Table 1. The surface of the Rh/V/SiO_2 system drops dramatically when the calcination temperature is raised from 973 to 1173 K. This has been reported previously (31, 32). In the Nb and Ta oxide promoted samples the surface shrinks by ca. 30% after calcination at 1173 K. The differences in the BET values of the HT calcined samples ($T_{calc} = 1173$ K) correlate with the melting point of the promoter oxides, V_2O_5 ($T_m = 963$ K), Nb_2O_5 ($T_m = 1793$ K), and Ta_2O_5 ($T_m = 2145$ K), respectively. In the Rh/V/SiO_2 samples, liquid V_2O_5 penetrates the pores and interparticle voids during the HT calcination. This effects a substantial sintering of the support as was demonstrated earlier by TEM (33).

The formation of crystalline mixed RhXO_4 was proven by XRD. After 573 and 773 K there is no crystalline phase detectable. Calcination at 973 K generates small amounts of $RhVO_4$ and $RhNbO_4$ besides V_2O_5 and Nb_2O_5, but no $RhTaO_4$ is formed. The formation of supported crystalline

TABLE 1

Specific BET Surface Areas of Rh/SiO_2, Rh/V/SiO_2, Rh/Nb/SiO_2, and Rh/Ta/SiO_2 after Calcination at 573, 773, 973, and 1173 K

Calcination temperature (K)	Specific BET surface areas (m^2/g)			
	Rh/SiO_2	Rh/V/SiO_2	Rh/Nb/SiO_2	Rh/Ta/SiO_2
573	366	289	302	242
773	357	281	261	244
973	409	179	266	257
1173	307	13	212	170

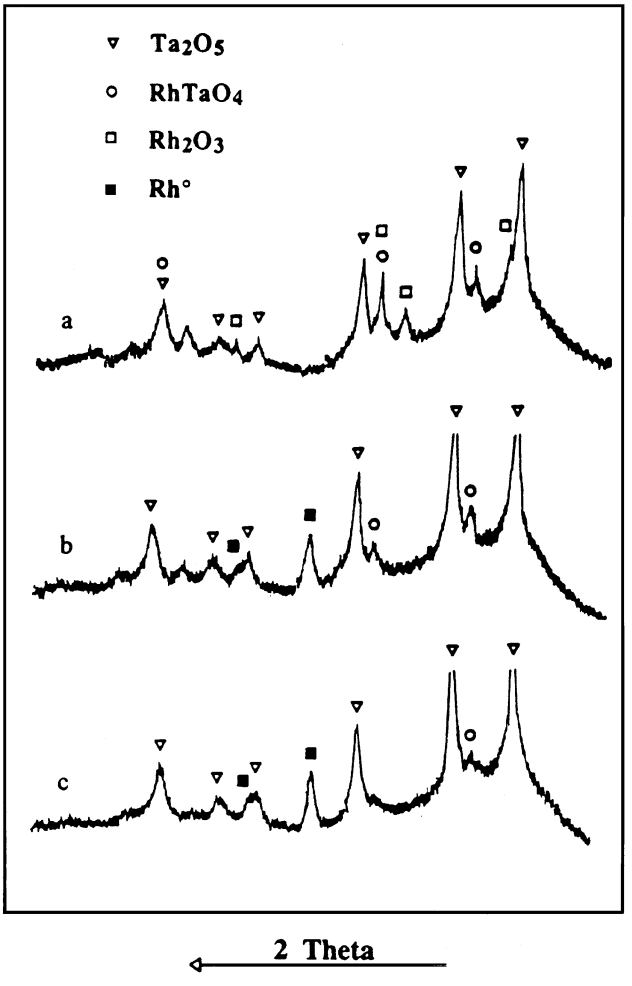

FIG. 1. Powder diffractions of Rh/Ta/SiO_2 after calcination at 1173 K (a) and H_2 reduction at 523 K (b) and 773 K (c).

$RhVO_4$ (27, 34, 35) and $RhNbO_4$ (18, 27, 34–36) has been described earlier. Further enhancement of the calcination temperature to 1173 K causes an increase in signal intensity for the V and Nb containing mixed oxide phases and leads to the appearance of small amounts of $RhTaO_4$ and Ta_2O_5 in Rh/Ta/1173 as shown in Fig. 1. In addition, bulk Rh_2O_3 is found in Rh/Ta/1173. An evaluation of the line width using the Scherrer formula points to Rh_2O_3 particles of 15 nm diameter, comparable to the unpromoted Rh/1173 catalyst. Powder diffraction data on $RhTaO_4$ are so far only available for unsupported $RhTaO_4$ (37).

Figure 2 displays the TPR profiles of Rh/SiO_2. They are almost identical to those reported earlier for comparable systems which were prepared from a $RhCl_3$ precursor (32). The H_2 consumptions at 366 and 342 K in Rh/573 and Rh/773, respectively, are typical for well dispersed rhodium oxide particles of about 2–3 nm diameter. Calcination at 973 or 1173 K leads to significant sintering of the metal oxide phase. This is reflected in a shift of the temperature of

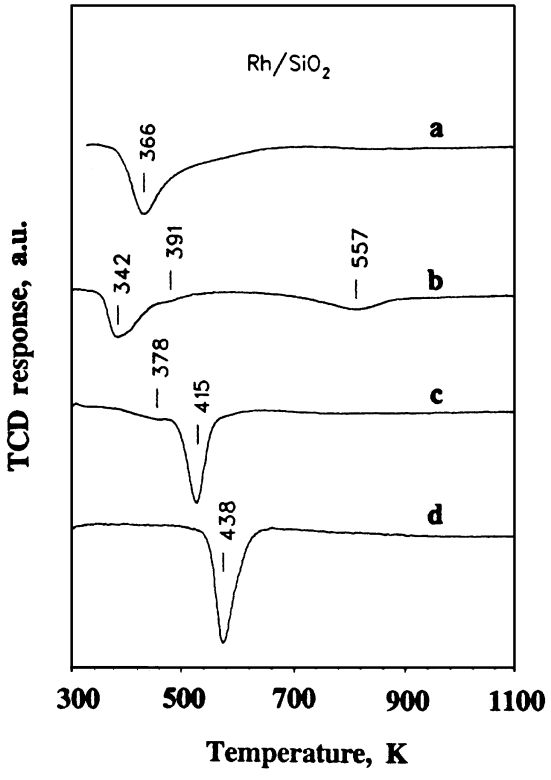

FIG. 2. TPR profiles of Rh/SiO_2 after calcination at 573 K (a), 773 K (b), 973 K (c), and 1173 K (d).

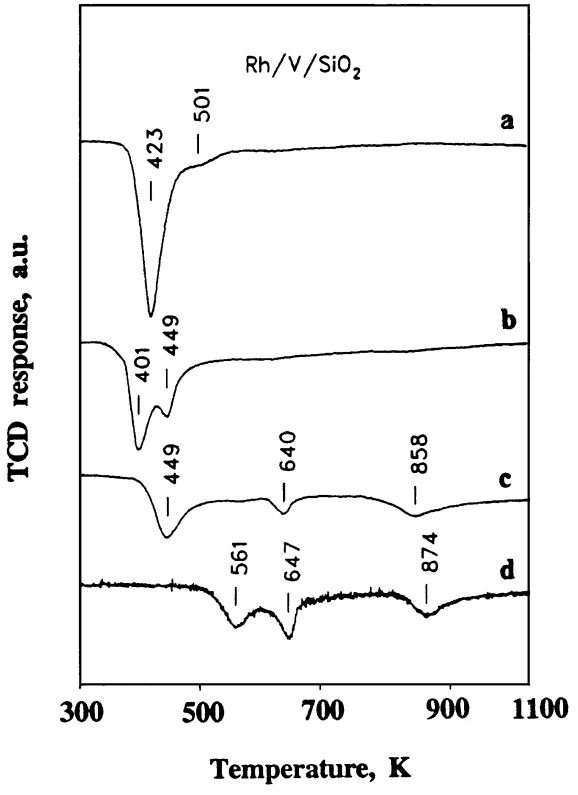

FIG. 3. TPR profiles of $Rh/V/SiO_2$ after calcination at 573 K (a), 773 K (b), 973 (c), and 1173 K (d).

maximum reduction rate, T_{max}, to 415 and 438 K for Rh/973 and Rh/1173, respectively. Figure 3 describes the reduction behavior of $Rh/V/SiO_2$. Again, the observed profiles are almost identical to those observed for systems prepared from the $RhCl_3$ precursor (32). H_2 consumptions below 500 K are attributed to the coreduction of Rh_2O_3 and V_2O_5. The overall hydrogen consumption corresponds to reduction of Rh^{3+} to Rh° and of V^{5+} to V^{3+}. The coincidence of these reduction processes is evidence of the simultaneous reduction of Rh^{3+} and V^{5+} ions. The high temperature shift of the reduction onset as compared to promoter free materials proves that this interaction results in a stabilization of the Rh_2O_3 phase by the promoter. TPR profiles of Rh/V/973 and Rh/V/1173 exhibit new signals at 640, and 561 and 647 K, respectively, which were ascribed to the formation of a bulk $RhVO_4$ phase. The high temperature peaks at 858 and 874 K were ascribed to reduction of bulk V_2O_5 which is not in contact with noble metal oxide. Note that calcination at 1173 K converts the rhodium precursor totally into $RhVO_4$.

Figure 4 shows the TPR profiles of $Rh/Nb/SiO_2$ after calcination at various temperatures. The shape and positions of the H_2 consumption peaks in the low temperature regime (up to 450 K) resemble those of the unpromoted Rh/SiO_2 catalysts. A very broad signal is observed at around 550 K in Rh/Nb/573. In $Rh/Nb/SiO_2$, calcined at 973 K, a new

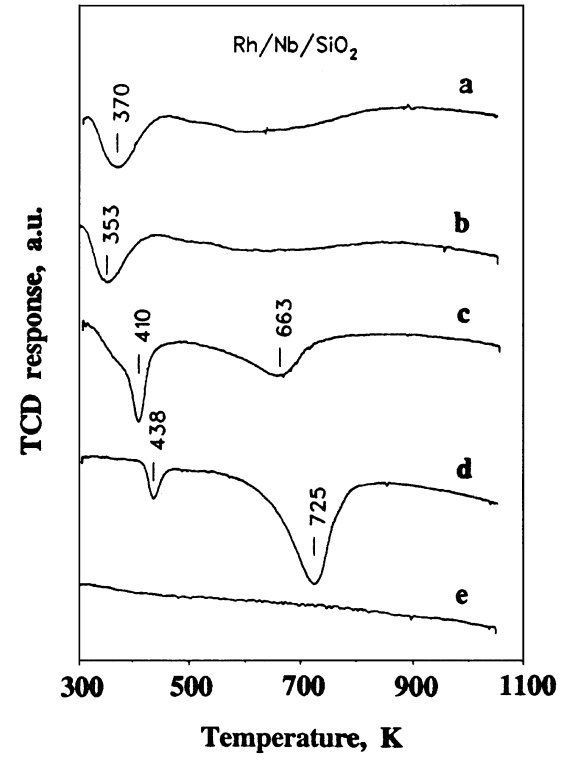

FIG. 4. TPR profiles of $Rh/Nb/SiO_2$ after calcination at 573 K (a), 773 K (b), 973 K (c), and 1173 K (d) and of Nb/573 (e).

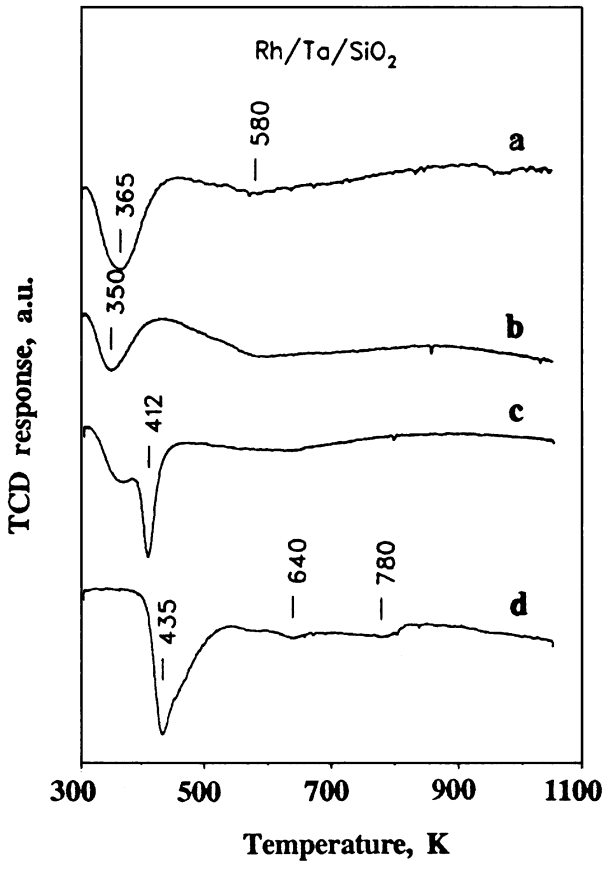

FIG. 5. TPR profiles of $Rh/Ta/SiO_2$ after calcination at 573 K (a), 773 K (b), 973 K (c), and 1173 K (d).

signal appears at 663 K. Increase in calcination temperature to 1173 K leads to an intensification and shift of this signal to 725 K. At the same time, signal intensity of the low temperature peak at 438 K becomes weaker.

TPR profiles of $Rh/Ta/SiO_2$ catalysts are depicted in Fig. 5. The low temperature features of all samples, again, coincide with those of unpromoted Rh/SiO_2. Similar to the niobia promoted Rh/SiO_2 catalysts, there are broad H_2 consumptions around 580 K in the low temperature calcined samples (profiles a and b). After calcination at 1173 K, additional weak signals appear at 640 and 780 K.

Reduced State

CO chemisorption capacities of unpromoted Rh/SiO_2 catalysts, calcined at 573 and 1173 K are presented in Table 2. As reported earlier, there is no influence of the reduction temperature, but a sharp decrease occurs after calcination at 1173 K which can be explained by sintering of the Rh_2O_3 phase (32, 38). The calculated particle sizes agree well with XRD and TEM data obtained earlier on corresponding catalysts with $RhCl_3$ precursors. Tables 3, 4, and 5 present the CO uptakes of $Rh/V/SiO_2$, $Rh/Nb/SiO_2$, and $Rh/Ta/SiO_2$ catalysts, respectively, after pretreatment at four different calcination temperatures and subsequent reduction at 523, 673, and 773 K. For V- and Nb-oxide promoted samples, the CO chemisorption capacity decreases with rising temperature of reduction for catalysts calcined at low temperature ($T_{calc} = 573$, 773 K). Such reduction induced SMSI effects have been found for similar catalysts (15, 39, 40). For V-promoted samples calcined at 973 and 1173 K, the CO uptakes are very low even after LT reduction as reported previously (33). As compared to pure Rh/SiO_2 samples, the CO chemisorption capacities are decreased by vanadium oxide, but increased by niobium oxide.

In contrast to $Rh/V/SiO_2$ and $Rh/Nb/SiO_2$, the CO uptake decreases for $Rh/Ta/SiO_2$ with severity of calcination and reduction pretreatments throughout the entire temperature ranges. Chemisorption capacities are still significant after calcination at 973 K and drop dramatically only in Rh/Ta/1173.

TABLE 2

CO Uptake, n_{CO}, Rhodium Dispersion, D, and Mean Rhodium Particle Diameter, d, of Rh/SiO_2 Calcined at 773 and 1173 K and Reduced at 523 and 773 K

Reduction temperature (K)	CO chemisorption capacity and mean Rh° particle diameter in Rh/SiO_2					
	Rh/773			Rh/1173		
	n_{CO} (μmol/g)	n_{CO}/Rh_t	d^a (nm)	n_{CO} (μmol/g)	n_{CO}/Rh_t	d^a (nm)
523	159	0.55	2.3	22	0.08	16.0
773	150	0.52	2.5	20	0.07	18.3

[a] Mean particle diameters were calculated using the formula $d = 6 \times \frac{V_M}{A_M} \times \frac{1}{D}$, where d is mean particle diameter; V_M, volume of a rhodium atom in the bulk with $V_M = M/\delta \times N_A$, where M is molecular weight of rhodium; δ, density of rhodium; N_A, Avogadro number; A_M, area of a rhodium atom on the surface (= 6.45 Å^2, value from Ref. (46)); D, dispersion with $D = Rh_s/Rh_t = n_{CO}/Rh_t$; Rh_s, number of surface atoms; Rh_t, total number of atoms.

TABLE 3

CO Chemisorption Capacities of $Rh/V/SiO_2$ Calcined at 573, 773, 973, and 1173 K and after reduction at 523, 673, and 773 K

Reduction temperature (K)	CO chemisorption capacity, n_{CO} (μmol/g), and rhodium dispersion, n_{CO}/Rh_t							
	Rh/V/573		Rh/V/773		Rh/V/973		Rh/V/1173	
	n_{CO}	n_{CO}/Rh_t	n_{CO}	n_{CO}/Rh_t	n_{CO}	n_{CO}/Rh_t	n_{CO}	n_{CO}/Rh_t
523	48	0.16	27	0.09	11	0.04	0	0.00
673	40	0.14	19	0.07	9	0.03	9	0.03
773	21	0.07	12	0.04	≤4	≤0.01	7	0.02

Note. n_{CO}, CO uptakes in μmol CO/g catalyst; n_{CO}/Rh_t, chemisorbed CO per total amount of Rh.

TABLE 4

CO Chemisorption Capacities of Rh/Nb/SiO_2 Calcined at 573, 773, 973, and 1173 K and after Reduction at 523, 673, and 773 K

Reduction temperature (K)	CO chemisorption capacity, n_{CO} (μmol/g), and rhodium dispersion, n_{CO}/Rh_t							
	Rh/Nb/573		Rh/Nb/773		Rh/Nb/973		Rh/Nb/1173	
	n_{CO}	n_{CO}/Rh_t	n_{CO}	n_{CO}/Rh_t	n_{CO}	n_{CO}/Rh_t	n_{CO}	n_{CO}/Rh_t
523	234	0.80	83	0.29	$\leq$4	$\leq$0.01	$\leq$4	$\leq$0.01
673	87	0.30	30	0.10	5	0.02	$\leq$4	$\leq$0.01
773	55	0.19	23	0.08	$\leq$4	$\leq$0.01	0	0.00

Note. n_{CO}, CO uptakes in μmol CO/g catalyst; n_{CO}/Rh_t, chemisorbed CO per total amount of Rh.

A thorough XRD characterization of the reduction behavior of Rh/V/SiO_2 as a function of the calcination temperature has been reported previously (27, 32, 33, 36). High metal dispersions were found for reduced samples which underwent calcination pretreatments in the range from 573 to 1173 K, but different reduction temperatures were needed for the generation of Rh° metal particles dependent on the severity of the previous calcination.

The Rh° metal particle sizes obtained after reduction of Rh/Nb/SiO_2 are comparable to those in the system Rh/V/SiO_2. For Rh/Nb/SiO_2 samples which were calcined at $T_{calc} \leq 973$ K and subsequently reduced at 523 K, XRD revealed the presence of highly dispersed Rh° particles of about 3 nm diameter. HT reduction leads only to a minor agglomeration of the noble metal particles. Reduction of $RhNbO_4$ as studied in Rh/Nb/1173, sets in at 573 K, but first traces of Rh° particles are detected only after reduction at 673 K. This is in agreement with results reported previously by Hu *et al.* (18) and Kunimori *et al.* (34). XRD signals for the mixed oxide phase disappear after H_2 treatment at 773 K with concomitant formation of Rh metal particles of sizes below 3 nm. Nb_2O_5 which was formed as well during calcination at 1173 K is not reduced at HT reduction. No crystalline NbO_2 is found in any of the HT reduced Rh/Nb/SiO_2 catalysts. A representative transmission electron micrograph of Rh/Nb/1173 after HT reduction is reproduced in Fig. 6. Elongated patches with round shaped edges which are composed of spherical particles with 2–3 nm diameter can be discerned. These structures resemble those of reduced $RhVO_4$ particles which have been reported previously (33).

TABLE 5

CO Chemisorption Capacities of Rh/Ta/SiO_2 Calcined at 573, 773, 973, and 1173 K and after Reduction at 523, 673, and 773 K

Reduction temperature (K)	CO chemisorption capacity, n_{CO} (μmol/g), and rhodium dispersion, n_{CO}/Rh_t							
	Rh/Ta/573		Rh/Ta/773		Rh/Ta/973		Rh/Ta/1173	
	n_{CO}	n_{CO}/Rh_t	n_{CO}	n_{CO}/Rh_t	n_{CO}	n_{CO}/Rh_t	n_{CO}	n_{CO}/Rh_t
523	240	0.82	173	0.59	62	0.21	8	0.03
673	190	0.65	123	0.42	46	0.16	$\leq$4	$\leq$0.01
773	124	0.43	71	0.24	46	0.16	$\leq$4	$\leq$0.01

Note. n_{CO}, CO uptakes in μmol CO/g catalyst; n_{CO}/Rh_t, chemisorbed CO per total amount of Rh.

The main difference in the reduction behavior of V- and Nb-oxide promoted Rh/SiO_2 which is apparent from XRD is related to the mixed oxide phases $RhVO_4$ and $RhNbO_4$, respectively. During reduction of $RhVO_4$ an intermediate was observed at $T_{red} = 523$ K (33). This phenomenon was rationalized by a two-step reduction of vanadium ions in $RhVO_4$, that is $V^{5+} \rightarrow V^{4+}$ and $V^{4+} \rightarrow V^{3+}$.

The reduction of Rh/Ta/573 and Rh/Ta/773 results in the formation of highly dispersed Rh° particles for both LT and HT reduction. These samples compare to the respective Nb promoted catalysts. Reduction of Rh/Ta/973 brings about small amounts of larger Rh° particles of 6–7 nm size. In Rh/Ta/1173, where bulk Rh_2O_3 has been observed in the oxidized state, large Rh° particles of 12 nm mean diameter are formed during LT reduction. Figure 1 shows that $RhTaO_4$ is reduced only after extended exposure to H_2 at 773 K for 2.5 h. No structures comparable to those of HT reduced $RhVO_4$ or $RhNbO_4$ were found in Rh/Ta/1173 after HT reduction as shown in the micrograph of Fig. 7. Instead, black spots between 10 and 20 nm diameter are seen which represent Rh° metal particles. Reduction at 773 K does not lead to a decrease in Ta_2O_5 peak intensity.

FTIR spectroscopy of adsorbed CO was used to probe cus sites on the promoter oxide surface at liquid nitrogen temperature. Figures 8, 9, and 10 show the carbonyl spectra of vanadium, niobium, and tanatalum oxide promoted Rh/SiO_2 catalysts, respectively, after different calcination pretreatments and reduction at 673 K. Two bands for CO adsorbed on cus promoter sites can be discerned in Rh/V/SiO_2 and Rh/Nb/SiO_2 samples. They are located at 2187 and 2178 cm^{-1} in Rh/V/SiO_2 and at 2191–2193 and 2177 cm^{-1} for Nb-promoted samples. The high frequency bands at 2187 and 2191–2193 cm^{-1}, respectively, increase in both groups with rising temperature of calcination, while the low frequency bands are dominant after calcination at 573 K. In order to evaluate band intensities, spectra A to D in Fig. 9 were decomposed into their components. The strong absorption bands at 2157 and 2133 cm^{-1} which are seen in Figs. 9 and 10 are readily attributed to H-bonded and physisorbed CO, respectively, on the silica surface (41). Shoulders in spectrum a were fitted with Gaussian functions and a FWHM of 17 cm^{-1}. Bands characteristic for H-bonded and physisorbed CO were fitted with Lorentzian functions. In contrast to vanadium and niobium oxide promoted Rh/SiO_2 catalysts, Rh/Ta/SiO_2 samples display only

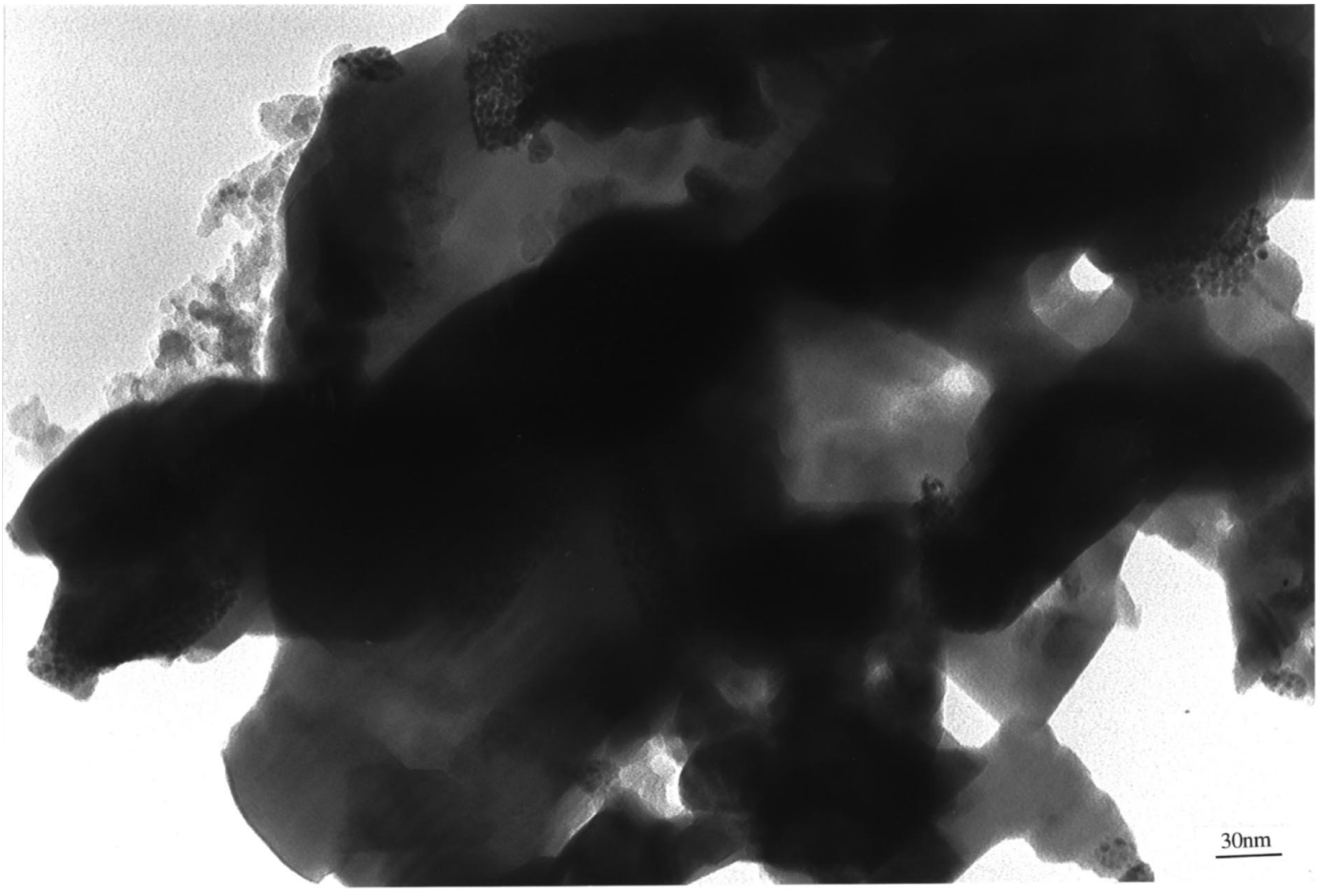

FIG. 6. TEM micrograph of Rh/Nb/1173 after 2 h reduction at 773 K.

one absorption band which shifts from 2193 to 2195 cm^{-1} with increasing calcination temperature.

DISCUSSION

Calcination Induced Metal–Promoter Interactions

(a) Calcination at 573 and 773 K. LT calcination ($T_{calc} =$ 573, 773 K) leads in all promoted systems $Rh/X/SiO_2$ to highly dispersed Rh_2O_3 particles which yield highly dispersed Rh° ($d < 3$ nm) metal particles after reduction. This is evident from XRD. The TPR profiles, however, differ for V-promoted catalysts as compared to Nb- and Ta-promoted ones. While the former reveals a blue-shift in the peak position and essentially coreduction of Rh^{3+} to Rh° and V^{5+} to V^{3+}, Nb- and Ta-promoted samples exhibit LT features reminiscent of those observed for unpromoted Rh/SiO_2 which are ascribed to reduction of Rh_2O_3 solely. The coincidence of signal positions for the LT reduction peaks in unpromoted and Nb- or Ta-promoted samples suggests similar Rh_2O_3 particle sizes. Unlike Rh/V/573 and Rh/V/773, there are broad H_2 consumption peaks in a temperature range between 500 and 800 K in the corresponding Nb and Ta containing catalysts. The integrated peak area of the low temperature signal at 370 K in Rh/Nb/573 corresponds to reduction of 80% of the noble metal oxide. The total H_2 consumption reveals a mean oxidation state of +4.8 for Nb, assuming complete reduction of Rh^{3+} to Rh°. It can be inferred that approximately 25% of the noble metal oxide is reduced only at temperatures higher than 500 K. The broad signal with peak maximum at 580 K is attributed to the reduction of highly dispersed Rh_2O_3 which is stabilized by cus sites of the promoter oxide. At the same time, around 20% of the Nb_2O_5 is reduced to NbO_2. Nb^{4+} cus sites are also found by FTIR spectroscopy. The two absorptions at 2191–2193 and 2177 cm^{-1} in Figs. 9A–9D are attributed to CO adsorbed on fivefold coordinated Nb^{5+} and Nb^{4+} sites, respectively. This interpretation is in agreement with a correlation that was established by Zaki and Knözinger (42) between stretching frequencies of CO adsorbed on cus sites and the electrostatic field strength of the adsorption site. The assignment of the high frequency band at

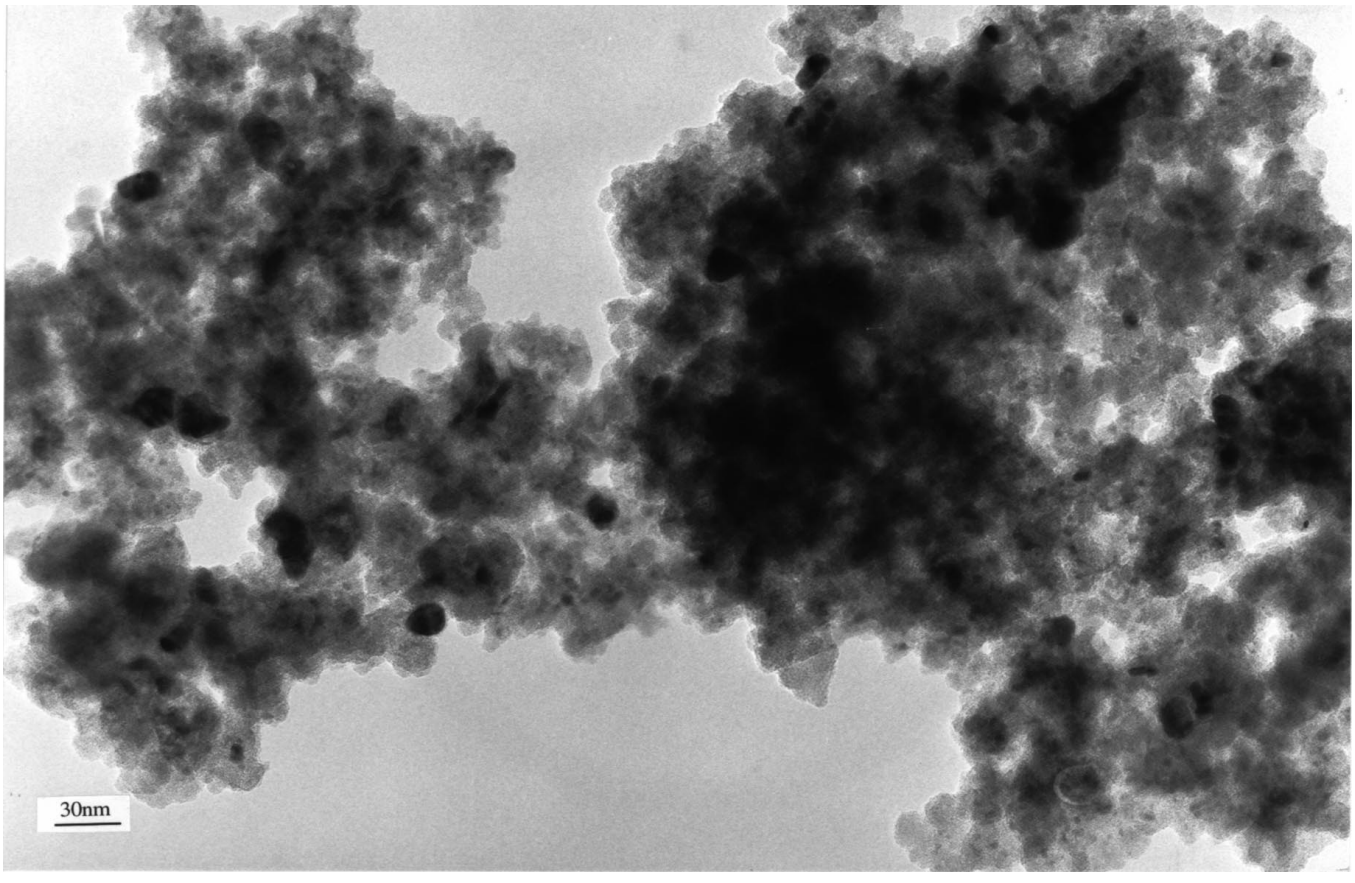

FIG. 7. TEM micrograph of Rh/Ta/1173 after 2 h reduction at 773 K.

2191–2193 cm^{-1} was confirmed by adsorption of CO on rhodium free Nb/SiO_2 calcined at 573 K. This sample gave rise to a single band for CO on cus sites at 2192 cm^{-1} in accordance with the presence of Nb_2O_5. The results obtained in this study are also in line with earlier data reported on silica supported niobia promoted rhodium catalysts (43, 44).

CO absorption bands close to 2178 and 2187 cm^{-1} which characterize $Rh/V/SiO_2$ have been found by Davydov *et al.* (45) in H_2 reduced silica supported vanadia and were ascribed to V^{3+} sites in slightly different coordination states. While fourfold coordinated trivalent vanadium ions are very likely responsible for the low frequency component, the band at 2187 cm^{-1} may equally be ascribed to a fivefold coordinated tetravalent vanadium site. Both vanadium and niobium oxide promoters are more easily reduced at lower calcination temperatures, and cus sites in their lower oxidation states, +4 for Nb and +3 for V, prevail.

In contrast to the Nb containing catalyst, TPR data of Fig. 5 suggest that Ta_2O_5 is not reduced to Ta^{4+} as the total H_2 consumption accounts for reduction of all Rh_2O_3 contained in the sample. The FTIR spectra of Fig. 10 display only one band between 2195 and 2193 cm^{-1}. This band is readily attributed to CO adsorbed on Ta^{5+} ions in fivefold coordination. The corresponding band for pure Ta/SiO_2 calcined at 973 K is situated at 2197 cm^{-1}. In contrast to $Rh/Nb/SiO_2$, no tetravalent oxidation state was detected for $Rh/Ta/SiO_2$. The stabilization of Rh_2O_3 in Rh/Ta/573 which is evident from the TPR profile a in Fig. 5 may result from an interaction of the noble metal oxide with pentavalent Ta oxide.

The CO chemisorption capacities of samples Rh/Nb/573 and Rh/Ta/573 measured after LT reduction are enhanced as compared to the unpromoted Rh/573 catalyst, while they are depleted in $Rh/V/SiO_2$. As the overall total activity in the CO hydrogenation reaction augments for all promoter elements, additional properties but the exposed metal surface have to play a role for the CO hydrogenation activity which is reported in a separate paper (46).

(b) Calcination at 973 and 1173 K. XRD patterns of promoted samples show that HT calcination induces the formation of mixed oxides $RhXO_4$. The amount of mixed oxide formed rises with temperature and decreasing atomic number of the promoter element. The existence of $RhXO_4$ is also evident from TPR. An H_2 consumption peak at

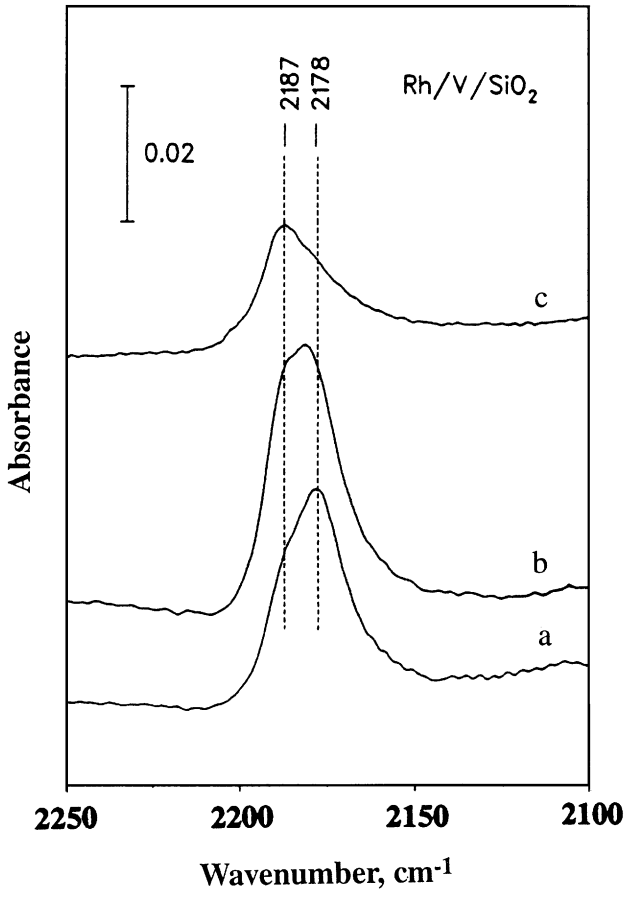

FIG. 8. FTIR spectra of the carbonyl stretching region after dosing 0.1 mbar CO at 85 K to Rh/V/573 (a), Rh/V/773 (b), and Rh/V/973 (c). Samples were *in situ* reduced at 673 K.

663 K in Rh/Nb/973 is ascribed to reduction of $RhNbO_4$. Hu *et al*. (27) observed H_2 consumption peaks between 680 and 800 K in Nb oxide promoted Rh/SiO_2 catalysts after calcination at 973 and 1173 K which were ascribed to $RhNbO_4$. The signal at 663 K is enhanced in intensity and shifted to 725 K after calcination at 1173 K in accordance with an increase in amount and particle size of $RhNbO_4$. Accordingly the signal intensity of unreacted Rh_2O_3 decreases. A quantitative evaluation of profiles c and d in Fig. 4 suggests that 50 and 90% respectively, of the noble metal have reacted to $RhNbO_4$. From signal integration it can be concluded that reduction of $RhNbO_4$ creates tetravalent Nb oxide. XRD and TEM prove that HT reduction of $RhNbO_4$ leads to well dispersed Rh° particles. The suppressed CO chemisorption capacity suggests that these particles are encapsulated in a matrix of Nb oxide. The stoichiometry of this matrix is NbO_2 according to TPR. Interestingly, the CO chemisorption capacity of Rh/Nb/973 is dramatically reduced after LT reduction although the metal dispersion is found to be high by XRD. The Rh° particle size is comparable to that in unpromoted Rh/773 sample for which a CO/Rh ratio of 0.55 was measured. As 50% of the noble metal in Rh/Nb/973 is present as Rh_2O_3 particles after calcination, a CO/Rh value in the range of 0.22 is expected after LT reduction. The very low CO uptake (CO/Rh = 0.01) indicates a strong metal oxide-promoter oxide interaction brought about by calcination. Calcination at 973 K possibly leads to a coverage of small Rh_2O_3 particles by Nb oxide. Subsequent H_2 treatment at LT results in reduction of the noble metal oxide which is still decorated by promoter oxide. The Nb oxide thus inhibits agglomeration of the Rh_2O_3 during calcination and suppresses chemisorption of CO on Rh° particles after LT reduction. This can be rationalized by assuming formation of a two-dimensional mixed oxide at the interface of Rh_2O_3 and Nb_2O_5 which can be considered the onset of the formation of bulk $RhNbO_4$. The possible interaction of noble metal and promoter oxide phases is visualized in Scheme 1.

In Rh/Ta/973 no distinct peak in the high temperature TPR regime is observed which is in line with the absence of crystalline $RhTaO_4$ in this sample. Small amounts of $RhTaO_4$ could be found only in Rh/Ta/1173 by XRD. The H_2 consumption peaks at 640 and 780 K in spectrum d of Fig. 5 are accordingly ascribed to reduction of $RhTaO_4$. According to TPR data, the promoter element is not reduced in $RhTaO_4$. The signal intensity of the reduction peak of Rh_2O_3 is essentially unchanged which is in line with the small amount of mixed oxide present in Rh/Ta/1173. Unlike Rh/Nb/973, the CO uptake of Rh/Ta/973 is still substantial, but significantly diminished compared to the unpromoted Rh/773 catalyst. Yet, Rh_2O_3 is well dispersed in Rh/Ta/973

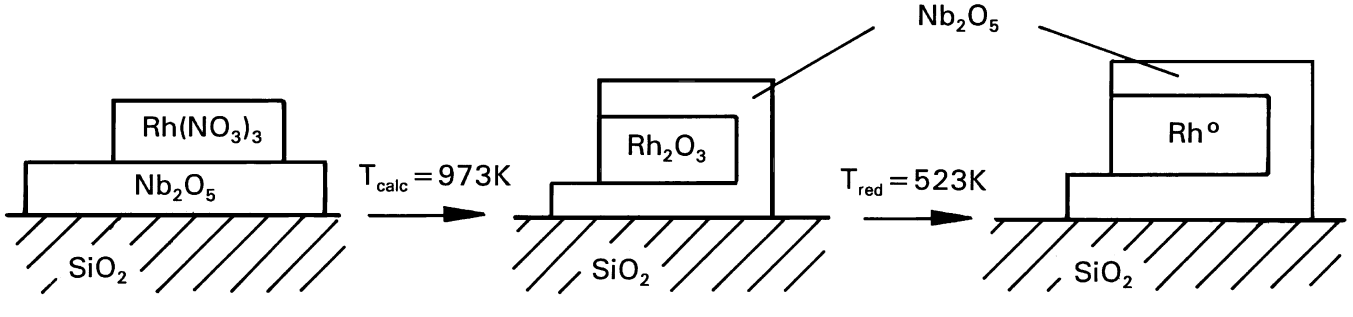

SCHEME 1

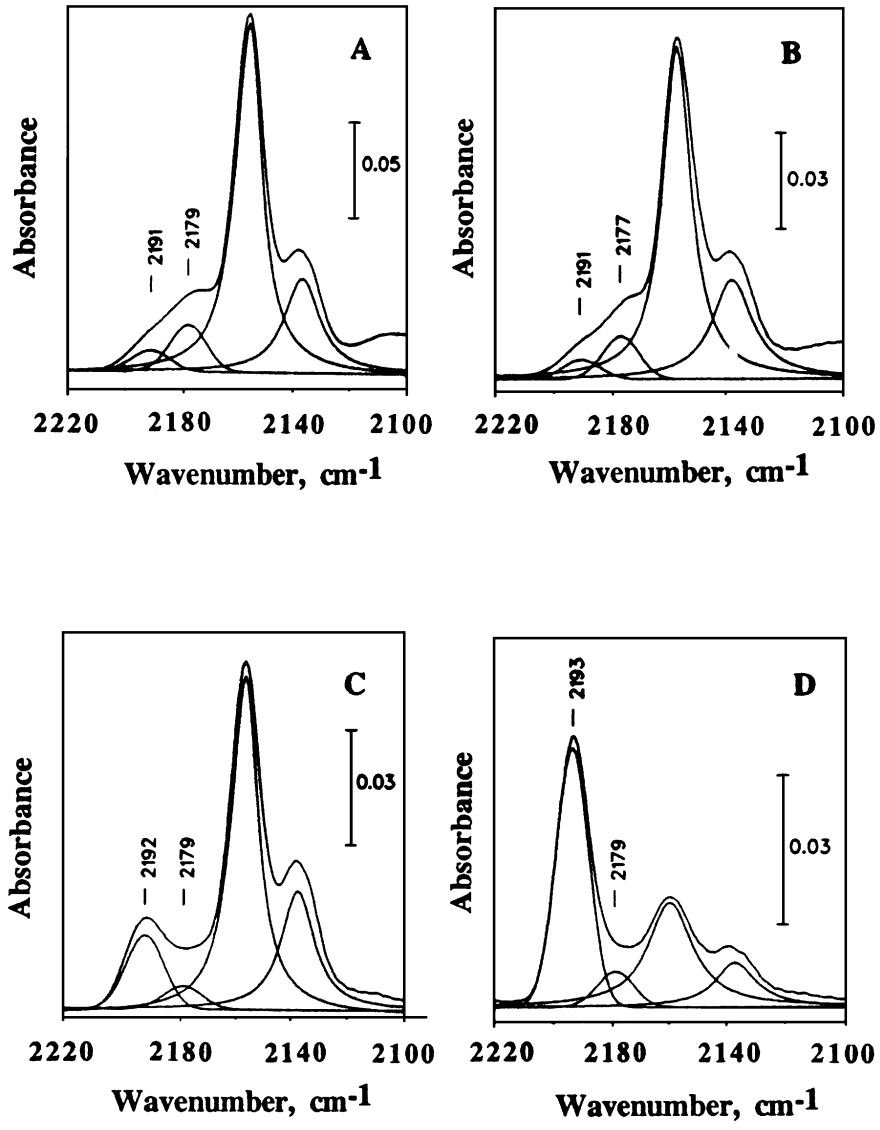

FIG. 9. FTIR spectra of Rh/Nb/573 (A), Rh/Nb/773 (B), Rh/Nb/973 (C), and Rh/Nb/1173 (D) after adsorption of 1 mbar CO at 85 K. Samples were reduced at 673 K.

and mainly small Rh° particles are formed during LT reduction. The reduced CO chemisorption capacity reflects probably a decoration of Rh_2O_3 by Ta oxide which is sustained during LT reduction. It appears that SMPI effects which were induced by HT calcination do not necessarily require reducible promoter oxides. While calcination induced SMPI effects occur with all Vb transition metal oxides its extent decreases in the order $V_2O_5 > Nb_2O_5 \gg Ta_2O_5$ according to the declining tendency toward formation of the respective $RhXO_4$ mixed oxides. As evident from TPR data, the peak maxima for the final reduction of $RhXO_4$ mixed oxides increases in the order V > Nb > Ta from 647 to 725 and 780 K, respectively. As these mixed oxides have the same structure, the lower reducibility of Rh^{3+} ions in $RhNbO_4$ and $RhTaO_4$ as compared to $RhVO_4$ parallels the higher stabilizing effect of the Nb and Ta promoter oxides on the reduction of Rh_2O_3 particles as observed in Figs. 3 and 4.

Reduction Induced Metal Promoter Interactions

HT treatment in H_2 is known to induce SMSI effects. A decrease in the CO uptake is also observed for Nb- and Ta-promoted Rh/SiO_2 catalysts after LT calcination and subsequent reduction to 673 or 773 K. From Tables 4 and 5 it is evident that this effect is less pronounced for $Rh/Ta/SiO_2$. Tauster and Fung (15) reported that SMSI effects are sluggish with Ta_2O_5 and reduction to 973 K was needed to extinguish the H_2 chemisorption capacity of Ta_2O_5 supported Ir catalysts.

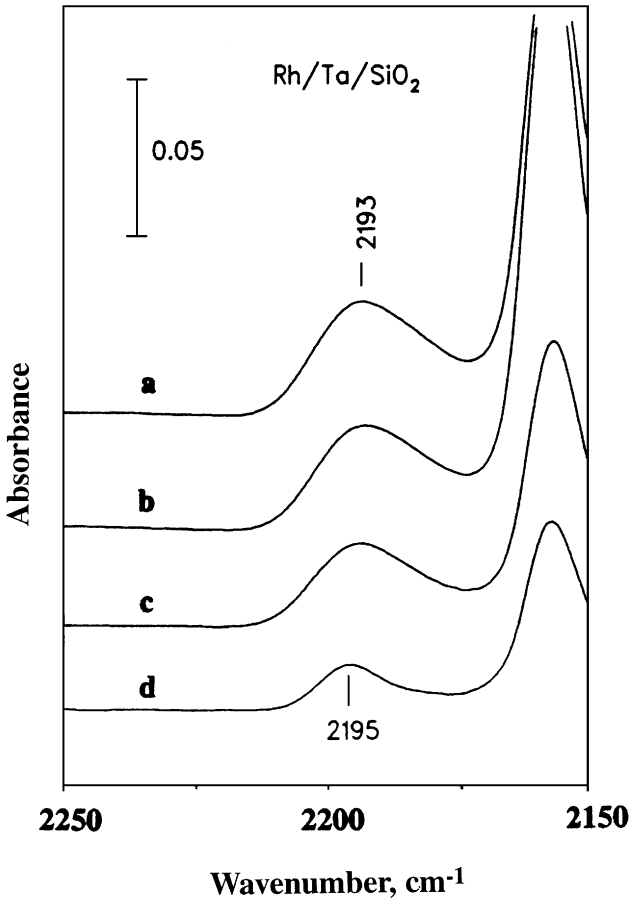

FIG. 10. FTIR spectra of Rh/Ta/573 (a), Rh/Ta/773 (b), Rh/Ta/973 (c), and Rh/Ta/1173 (d) after adsorption of 1 mbar CO at 85 K. Samples were reduced at 673 K.

In the HT calcined samples the formation of crystalline $RhXO_4$ (X = Nb, Ta) is observed in Rh/Nb/973 and Rh/Ta/1173 by XRD. These mixed oxides are not reduced by H_2 treatment at 523 K, but only between 673 and 773 K. It has been shown earlier that reduction of $RhVO_4$ leads to well dispersed Rh° particles embedded in a matrix of V_2O_3. The CO uptake in Rh/V/973 and Rh/V/1173 was accordingly found to be very low. The amount of mixed oxide formed decreases in the order $RhVO_4 > RhNbO_4 \gg RhTaO_4$. The CO chemisorption capacity is low in Rh/Nb/973 and Rh/Ta/1173 despite of the lesser abundance of mixed oxides in these samples. This low CO uptake is observed after LT reduction and can be explained by a decoration of Rh_2O_3 with Nb oxide in Rh/Nb/973 and by the formation of large Rh_2O_3 particles in Rh/Ta/1173, respectively. As both effects are induced by calcination, there is no difference in CO uptake as reduction conditions become more severe.

CONCLUSIONS

Metal–promoter oxide interactions were studied in Rh/SiO_2 catalysts promoted with Vb transition metal oxides. Different interactions were induced by HT reduction ($T_{red} \geq 673$ K) with and without previous HT calcination ($T_{calc} \geq 973$ K). HT calcination leads to formation of mixed oxides $RhXO_4$ of the same rutile type structure. The amount of formed mixed oxide decreases in the order $RhVO_4 > RhNbO_4 \gg RhTaO_4$. HT reduction of $RhXO_4$ generates highly dispersed Rh° metal particles embedded in a matrix of promoter oxide. The promoter elements V and Nb in these mixed oxides are reduced from oxidation states +5 to +3 and from +5 to +4, respectively, but no reduction of Ta^{5+} ions is observed. The depth of reduction is reflected in the reducibility of these mixed oxides which decreases in the order $RhVO_4 \gg RhNbO_4 > RhTaO_4$.

Strong metal promoter oxide interactions as indicated by a strong decrease of the CO chemisorption capacity were detected for V and Nb containing samples even after LT reduction ($T_{red} = 523$ K) if the samples were calcined at 973 K prior to reduction. This effect is less pronounced for the Ta oxide promoted catalyst. In the calcination induced SMPI state, small Rh° metal particles are covered by promoter oxide. Less reducible oxides Nb_2O_5 and Ta_2O_5 remain in their original oxidation states. This HT calcination effected metal–promoter oxide interaction results presumably from the onset of mixed oxide formation at the metal oxide–promoter oxide interface.

ACKNOWLEDGMENTS

This work was financially supported by the Deutsche Forschungsgemeinschaft in the framework of the Sonderforschungsbereich 338 and by the Fonds der chemischen Industrie. A gift of tantalum oxalate solution from HCST is gratefully acknowledged.

REFERENCES

1. Van Santen, R. A., "Fundamental Aspects of Heterogeneous Catalysis Studied by Particle Beams" (H. H. Brongersma and R. A. van Santen, Eds.), p. 83. Plenum, New York, 1991.
2. Sheu, L. L., Knözinger, H., and Sachtler, W. M. H., *J. Am. Chem. Soc.* **111**, 8125 (1989).
3. Lin, Y. J., Resasco, D. E., and Haller, G. L., *J. Chem. Soc. Faraday Trans.* **83**, 2091 (1987).
4. Kowalski, J., van der Lee, G., and Ponec, V., *Appl. Catal.* **19**, 423 (1985).
5. Kip, B. J., Hermans, E. G. F., and Prins, R., *Appl. Catal.* **35**, 423 (1985).
6. Koerts, T., Welters, J. J., and van Santen, R. A., *J. Catal.* **134**, 1 (1992).
7. Mori, T., *Catal. Lett.* **7**, 151 (1990).
8. Boffa, A. B., Bell, A. T., and Somorjai, G. A., *J. Catal.* **139**, 602 (1993).
9. Onishi, H., Aruga, T., Egawa, C., and Iwasawa, Y., *Surf. Sci.* **233**, 261 (1990).
10. Sachtler, W. M. H., *Proc. 10. Simp. Iberoamer. Catálisis, Merida* **2**, 1327 (1986).
11. Crowell, J. E., Garfunkel, E. L., and Somorjai, G. A., *Surf. Sci.* **121**, 303 (1982).
12. Herrmann, J.-M., and Pichat, P., *J. Catal.* **78**, 425 (1982).
13. Yakovlev, A. L., Zhidomirov, G. M., Neyman, K. M., Nashizov, V. A., and Rösch, N., *Ber. Bunsenges. Phys. Chem.* **100**, 413 (1996).
14. Tauster, S. J., Fung, S. C., and Garten, R. L., *J. Am. Chem. Soc.* **100**, 170 (1978).

15. Tauster, S. J., and Fung, S. C., *J. Catal.* **55**, 29 (1978).
16. Logan, A. D., Braunschweig, E. J., Datye, A. K., and Smith, D. J., *Langmuir* **4**, 827 (1988).
17. Yao, M. H., "Proceedings, 51th Annual Meeting of the Microscopy Society of America" (G. W. Bailey and C. L. Rieder, Eds.), p. 734. San Francisco Press, San Francisco, 1993.
18. Hu, Z., Nakamura, H., Kunimori, K., Yokoyama, Y., Asano, H., Soma, M., and Uchijima, T., *J. Catal.* **119**, 33 (1989).
19. Kip, B. J., Smeets, P. A. T., van Wolput, J. H. M. C., Zandbergen, H. W., van Grondelle, J., and Prins, R., *Appl. Catal.* **33**, 157 (1987).
20. Tauster, S. J., *Acc. Chem. Res.* **20**, 389 (1987).
21. Haller, G. L., and Resasco, D. E., *Adv. Catal.* **36**, 173 (1989); *J. Catal.* **82**, 279 (1983).
22. Van der Lee, G., Schuller, B., Post, H., Favre, T. L. F., and Ponec, V., *J. Catal.* **98**, 522 (1986).
23. Tomczak, D. C., Zhobolenko, V. L., Treviño, H., Lei, G.-D., and Sachtler, W. M. H., *in* "Zeolites and Related Microporous Materials: State of the Art 1994" (J. Weitkamp, H. G. Karge, H. Pfeifer, and W. Hölderich, Eds.), p. 893. Elsevier, Amsterdam. 1994.
24. Kunimori, K., Wakasugi, T., Yamakawa, F., Oyanagi, H., Nakamura, J., and Uchijima, T., *Catal. Lett.* **9**, 331 (1991).
25. Kunimori, K., Oyanagi, H., Shindo, H., Ishigaki, T., and Uchijima, T., "Proceedings, 10th International Congress on Catalysis, Budapest, 1992" (L. Guczi, F. Solymosi, and P. Tetenyi, Eds.), p. 2039. Akadémiai Kiadó, Budapest, 1993.
26. Hu, Z., Wakasugi, T., Maeda, A., Kunimori, K., and Uchijima, T., *J. Catal.* **127**, 276 (1991).
27. Hu, Z., Nakamura, H., Kunimori, K., Asano, H., and Uchijima, T., *J. Catal.* **112**, 47 (1988).
28. Linsmeier, Ch., Dissertation, Univ. München, 1994.
29. Heal, G. R., and Mkayula, L. L., *Carbon* **26**, 815 (1988).
30. Kunzmann, G., Dissertation, Univ. München, 1987.
31. Del Arco, M., Holgado, M. J., Martin, C., and Rives, V., *Langmuir* **6**, 801 (1990).
32. Beutel, T., Knözinger, H., Siborov, A. V., and Zaikovskii, V. I., *J. Chem. Soc. Faraday Trans.* **88**, 2775 (1992).
33. Tesche, B., Beutel, T., and Knözinger, H., *J. Catal.* **149**, 100 (1994).
34. Kunimori, K., Hu, Z., Uchijima, T., Asakura, K., Iwasawa, Y., and Soma, M., *Catal. Today* **8**, 85 (1990).
35. Yin, Y. G., Wakasugi, T., Shindo, H., Ito, S., Kunimori, K., and Uchijima, T., *Catal. Lett.* **9**, 43 (1991).
36. Kunimori, K., Shindo, H., Oyanagi, H., and Uchijima, T., *Catal. Today* **16**, 387 (1993).
37. Prosychev, I. I., Lazarev, V. B., and Shaplygin, I. S., *J. Inorg. Chem.* **26**, 413 (1981).
38. Wong, C., and McCabe, R. W., *J. Catal.* **119**, 47 (1989).
39. Kunimori, K., Abe, H., and Uchijima, T., *Chem. Lett.* 1619 (1983).
40. Yoshitake, H., Asakura, K., and Iwasawa, Y., *J. Chem. Soc. Faraday Trans. 1* **84**, 4337 (1988).
41. Beebe, T. P., Gelin, P., and Yates, J. T., Jr., *Surf. Sci.* **148**, 526 (1984).
42. Zaki, M., and Knözinger, H., *Spectrochim. Acta* **43A**, 1455 (1987).
43. Kraus, L., Zaki, M. I., Knözinger, H., and Tesche, B., *J. Mol. Catal.* **55**, 55 (1989).
44. Alekseev, O. A., Beutel, T., Paukshtis, E. A., Ryndin, Yu. A., and Knözinger, H., *J. Mol. Catal.* **92**, 217 (1994).
45. Davydov, A. A., Budneva, A. A., and Maksimov, N. G., *React. Kinet. Catal. Lett.* **20**, 93 (1982).
46. Scholten, J. J., Pijpers, A. P., and Hustings, A. M. L., *Catal. Rev. Sci. Eng.* **27**, 151 (1985).